

Green Chemistry

Accepted Manuscript



This is an *Accepted Manuscript*, which has been through the Royal Society of Chemistry peer review process and has been accepted for publication.

Accepted Manuscripts are published online shortly after acceptance, before technical editing, formatting and proof reading. Using this free service, authors can make their results available to the community, in citable form, before we publish the edited article. We will replace this *Accepted Manuscript* with the edited and formatted *Advance Article* as soon as it is available.

You can find more information about *Accepted Manuscripts* in the [Information for Authors](#).

Please note that technical editing may introduce minor changes to the text and/or graphics, which may alter content. The journal's standard [Terms & Conditions](#) and the [Ethical guidelines](#) still apply. In no event shall the Royal Society of Chemistry be held responsible for any errors or omissions in this *Accepted Manuscript* or any consequences arising from the use of any information it contains.



www.rsc.org/greenchem



Green Chemistry

PAPER

In-situ Synthesis of Two-dimensional Leaf-like $\text{Cu}_2\text{ZnSnS}_4$ Plate Arrays as Pt-free Counter Electrode for Efficient Dye-Sensitized Solar Cells

Received 00th January 20xx,
Accepted 00th January 20xx

DOI: 10.1039/x0xx00000x

www.rsc.org/

Shan-Long Chen,^{ab} Ai-Chun Xu,^a Jie Tao,^{a*} Hai-Jun Tao,^{ab} Yi-Zhou Shen,^a Lu-Min Zhu,^a Jia-Jia Jiang,^a Tao Wang^a and Lei Pan^a

Kesterite-structure $\text{Cu}_2\text{ZnSnS}_4$ (CZTS) has been proved to be a high-performance Pt-free counter electrode (CE) material for dye-sensitized solar cells (DSSCs). Herein, a green but powerful two-step method based on solvothermal treatment was proposed to synthesize semi-transparent two-dimensional (2D) leaf-like CZTS plate arrays (PLAR) in situ on FTO glass substrate, without any post-treatments, such as annealing, toxic sulfurization, or coating with other ancillary materials. The growth mechanism of the 2D leaf-like CZTS PLAR based on solvothermal treatment was illustrated. Power conversion efficiency (PCE) of 7.09 % was obtained by utilizing leaf-like CZTS PLAR as CE. Surprisingly, PCE increased to 8.67 % assisted by a mirror reflection. The excellent performance of DSSCs could be attributed to high catalytic surface area, fast photo-generated electron transport at the counter electrode/redox electrolyte interface, remarkable electrocatalytic activity for I_3^- reduction, low charge transfer resistance toward the reduction of I_3^- ions, and high diffusion coefficient of the I_3^- . This work provides a green and feasible approach to construct high-quality metal sulfide nanoarrays on arbitrary conductive substrates under mild condition (i.e. low temperature, no annealing, environment, speediness) and promotes the development of Pt-free sulfide materials for sustainable photovoltaic applications.

Introduction

Under the threat of global warming and energy crises, the utilization of green/renewable energy is becoming more and more essential.^{1,2} Thin-film sensitized solar cells (dye-sensitized solar cells (DSSCs)) have attracted many attentions due to their advantages of environmental friendliness, high-throughput manufacturing methods, potentially low production costs, and relatively high efficiency ($\eta=13\%$).²⁻⁶ Basically, typical DSSCs have a sandwich-type structure, consisting of a platinized fluorine-doped tin oxide (FTO) glass as the counter electrode (CE), a liquid electrolyte that traditionally contains I^-/I_3^- redox couples as a conductor to electrically connect the two electrodes, and a porous-

structured oxide film adsorbed with dye molecules as the photosensitized anode.^{6,7} As an essential and crucial component in DSSCs, the counter electrode (CE) behaves as a catalyst for the redox couples regeneration in the electrolyte, as well as an electron collector from the external circuit. The CE materials should possess two advantages of high catalytic activity and electrical conductivity.⁸ Generally, platinum (Pt) deposited on a transparent conducting oxide (TCO) such as indium tin oxide (ITO) or fluorine-doped tin oxide (FTO) is usually employed as the CE for DSSCs, presenting high catalytic activity, high efficiency and long-term stability.⁹ However, the high cost and low natural abundance of Pt have been a major concern. Furthermore, Pt can be dissolved in the iodine electrolyte solution and decomposed to unwanted PtI_4 and H_2PtI_6 by-products in the long term.¹⁰ Hence, to address the problem of high cost and instability for Pt CE, many alternative Pt-free materials have been proposed to be used as CE catalysts, including carbon materials (carbon black,¹¹ graphite,¹² carbon nanotubes,¹⁰ graphene,¹¹ etc.), conducting polymers (polyaniline, poly-(3,4-ethylene dioxythiophene) (PEDOT), etc.), and the inorganic compounds (transition metal in the form of oxides, nitrides, carbides, and sulfides^{8,10,13,14}). In recent years, p-type kesterite-structure $\text{Cu}_2\text{ZnSnS}_4$ (CZTS) has been proved to be a high catalytic CE material, due to its advantages of earth abundance (Pt: 0.0037 ppm, Cu: 50 ppm, Zn: 75 ppm, Sn: 2.2 ppm), low-toxicity, a direct band gap of 1.5 eV, and excellent catalytic ability towards I_3^- electrolyte. The performance of the DSSCs with CZTS is comparable to that of

^a College of Material Science and Technology, Nanjing University of Aeronautics and Astronautics, Nanjing 210016, P R China. E-mail: taojie@nuaa.edu.cn; Tel: (+86) 025-5211 2911.

^b Jiangsu Province Key Laboratory of Materials and Technology for Energy Conversion, Nanjing University of Aeronautics and Astronautics, Nanjing 210016, P R China. E-mail: Shanlongchen@nuaa.edu.cn; Tel: (+86) 025-5211 2911.

† Footnotes relating to the title and/or authors should appear here.

Electronic Supplementary Information (ESI) available: 2D and 3D AFM images of CZTS particles film and leaf-like CZTS plate arrays, FE-SEM images, Raman spectra of nano-rounded CZTS sheet arrays on FTO substrate, and TEM images of the nano-rounded CZTS sheet, HR-TEM image of a single nano-rounded sheet scraped from the films of CZTS arrays, Magnified FE-SEM image of a single CZTS plate with the rough pointed cone covering on the surface, Comparison with the photoelectrochemical performance of DSSCs using various counter electrode (CE). See DOI: 10.1039/x0xx00000x

the cell with Pt, indicating the high potential for CZTS to replace Pt in DSSCs.¹⁴ Many approaches have been developed to fabricate CZTS thin film counter electrode, such as vacuum based deposition (pulsed laser deposition, evaporation and sputtering), chemical vapour deposition, electrodeposition, and solution-based processing (solvothermal or hot-inject method to synthesize the CZTS nanoparticles with post coating and sulfurization). The related CZTS-based device properties of the above reports are summarized in Table S1. However, most of the aforementioned researches were focusing on the special morphology construction, high crystallization, and super catalytic activity towards the reduction of the ions in electrolytes. It is unavoidably to apply rigorous synthesis techniques, such as high vacuum condition, high annealing temperature (300 °C-600 °C), using excessive, expensive and toxic organic ligands to control the unique morphology, adopting multiple steps (CZTS inks spin/spray coating with post annealing, more than 12 h solvothermal synthesis), and requiring toxic sulfur source (H₂S or sulfur vapour), to meet the above goals.¹⁴⁻²² In addition, the flexible DSSCs based on conducting polymers as a substrate cannot bear beyond 150 °C heat treatment.²² There are no reports on fabricating the nanostructured CZTS thin film in situ on conductive substrate through solution-based processing without any post-treatments (annealing or sulfurization). Thus, it is necessary to develop a simple, cost-effective, green, and in-situ mild synthesis method for good-crystallinity, good-stability, and high-performance CZTS thin film for DSSCs application.

Herein, we propose a facile, green but powerful solution method to synthesize semi-transparent two-dimensional (2D) leaf-like CZTS plate arrays (PLAr) in situ on FTO glass substrate and use it directly as CE to assemble DSSCs without any post-treatments, such as annealing, sulfurization, or coating with other ancillary materials. The Cu-Zn-Sn alloy composites were firstly electrodeposited on a FTO substrate and then were converted to CZTS directly by a novel solvothermal treatment at low temperature and short reaction time. It is noteworthy that, as mentioned in previous reported papers, the conventional solvothermal method was always adopted to synthesize nanostructured CZTS powders, not to fabricate the CZTS thin film CE directly on substrate. Furthermore, sulfurization or post heat treatment was essential to acquire the CZTS CE with good adhesion, high crystallization, and super catalytic activity, if the CZTS precursor film was obtained before. There are no reports on the synthesis of pure kesterite-structure CZTS thin film directly on FTO substrate at 200 °C or below 300 °C. The solvothermal-obtained leaf-like CZTS PLAr film has good bonding strength, high catalytic surface area, high carrier mobility at the CE/electrolyte interface, and superior catalytic activity toward the reduction of I₃⁻/I⁻ ions. The 2D CZTS electrode was introduced as CE for DSSCs to achieve 7.09 %, higher than that of Pt CE. Surprisingly, when a mirror was placed under the testing cell, the PCE increased to 8.67 %. Our results demonstrate the effectiveness of the in-situ solvothermal treatment to the construction of

various sulfide-based nanostructures thin film for the green energy applications in DSSCs, as well as photocatalytic hydrogen generation, supercapacitor, and lithium ion batteries.

Experimental Section

Materials

Copper (II) sulfate pentahydrate (CuSO₄·5H₂O), ethanol, and acetonitrile were obtained from Sinopharm Chemical Reagent Co., Ltd. (Shanghai, China) in analytical purity. Tin (II) sulfate (SnSO₄), zinc (II) sulfate monohydrate (ZnSO₄·H₂O), sodium citrate dihydrate (Na₃C₆H₇O₆·2H₂O), lithium perchlorate (LiClO₄), lithium iodide (LiI), and iodine were purchased from Aladdin Industrial Corporation (China) in analytical purity. J & K Scientific Ltd. (Shanghai, China) provided the sulfur in sublimed grade (99.5%). FTO glass (sheet resistance 7-8 Ω sq⁻¹), N719 dye (0.3 mM (Bu₄N)₂[Ru(dcbpyH)₂(NCS)₂]), and electrolyte (DHS-Et23) were obtained from OPV Tech Co., Ltd (China), Dyesol (Australia), and HeptaChroma (China) respectively. All chemicals in the experiments were used as received. Distilled water was used throughout the work.

Fabrication of CZTS plate arrays counter electrodes (CEs)

A semi-transparent film of CZTS plate arrays was in-situ grown on a FTO glass substrate, first by using electrodeposition followed by adopting a novel solvothermal treatment (as shown in Figure 1). In the electrodeposition process, metallic precursors of Cu, Sn, and Zn (CZT) films were electrodeposited on an FTO glass substrate simultaneously. The CZT composite layer was deposited at -1.17 V (vs. SCE) for 60 s using an electroplating bath containing 3.5 mM copper sulfate pentahydrate (CuSO₄·5H₂O), 2.1 mM tin sulfate (SnSO₄), 20 mM zinc sulfate monohydrate (ZnSO₄·H₂O), and 50 mM sodium citrate dihydrate (Na₃C₆H₇O₆·2H₂O). The deposition temperature was kept at 22 °C and the exposed geometric area of FTO substrate (2×1.5 cm²) was 1.5×1.5 cm². After electrodeposition, the CZT precursor film was soaked in distilled water and dried at 70 °C in air. The obtained CZT film on the FTO was converted to the CZTS film via a novel solvothermal treatment. In a typical solvothermal treatment, the CZT film (with the conductive area facing down), 35 ml ethanol and 2 mM (0.0641 g) excessive sulfur powders were put into a 50 ml Teflon-lined autoclave successively. The autoclave was then maintained at 200 °C until the CZT precursor film had been reacted in adequate. Various reaction periods (i.e., 1 h, 3 h, and 6 h) were used for the investigation of conversion process. After conversion process, the obtained dark brown film was washed with ethanol and dried at 70 °C. Finally, CZT particles film on FTO was converted to leaf-like CZTS plate arrays (PLAr) without any post heat treatment. Pt CE was purchased from Dyesol (Australia) for comparison.

Assembly of the DSSCs

For a fair comparison, all the DSSCs were fabricated with TiO₂ photoanode materials relying on a standardized fabrication process. Firstly, the clean FTO substrate was subjected to TiCl₄ aqueous solution (0.05 M) treatment for the duration of 30 min at 70 °C. A commercial TiO₂ paste (P25, Degussa, Germany) was then coated on above pre-treated FTO substrate by doctor blading method. A portion of 0.20 cm² was selected as the active photo-anode area. The TiO₂-coated FTO glasses were gradually heated to 500 °C (rate=2 °C/min) in air and subsequently sintered at that temperature for 30 min to create TiO₂ film. The total thickness of the TiO₂ film was about 18 μm. After the heat treatment, the substrate was subjected to TiCl₄ aqueous solution treatment again to acquire more dye absorbing. Thereafter, the 80 °C baked electrode was immersed in solution, containing 0.3 mM N719 dye in anhydrous ethanol for 24 h at room temperature under dark condition. The TiO₂ electrode was coupled with one of the various CEs (CZTS and commercial Pt) to fabricate the DSSCs. The electrolyte was injected into the gap between the two electrodes by capillarity, and the hole was sealed with hot-melt glue after the electrolyte injection.

Characterization

The crystalline phase and purity of CZTS samples were examined by a X-ray diffractometer (RIGAKU, Smartlab TM9 KW, Cu Kα radiation at λ=1.541 Å,) operated at 40 kV/200 mA, and a confocal Raman microscope (Renishaw, inVia) using the 488 nm laser line of an air cooled Ar-ion laser. The optical images were taken by digital camera. The morphologies of synthesized nanostructures were observed by using field-emission-scanning electron microscopy (FE-SEM, HITACHI, SU-4800) and atomic force microscopy (AFM, Bruker, Dimension Icon). Energy-dispersive spectroscopy (EDS) from FE-SEM was used for the elemental analysis of the CZTS films. The detailed nanostructures and crystal structure were further investigated by a transmission electron microscopy (TEM, FEI Tecnai G2), coupled with selected area electron diffraction (SAED) and EDS mapping. The thin films were scraped from their substrates and dispersed in ethanol to form the suspensions for TEM observation. The assembled DSSCs were illuminated by a solar simulator (94042A, AM1.5 G, Newport, America), and the incident light intensity (100 mW/cm²) was calibrated with a standard Si cell (91150V, Newport, America), so as to measure the J-V curves of the solar cells devices. The Cyclic voltammetric (CV) measurements were performed at a scan rate of 100 mV s⁻¹ in acetonitrile solution consisting of 10 mM LiI, 1 mM I₂, and 0.1 M LiClO₄ in a three-electrode system, by using CHI 660E potentiostat, in which the as-fabricated CEs acted as the working electrode, in addition to a Pt sheet (6 cm²) counter electrode and a Ag/Ag⁺ (CHI 112) couple served as a reference electrode. Tafel polarization curves were obtained using symmetrical cells, at 10 mV s⁻¹, using a CHI 660E

potentiostat with a two-electrode system. The symmetrical cell contained two identical electrodes and the film area was confined to be 0.25 cm². The two electrodes were separated by a 60 μm thick Teflon tape. The EIS tests of the symmetric thin layer CEs were carried out in the frequency ranging from 0.05 to 10⁶ Hz at 0 V bias with perturbation amplitude of 5 mV, under dark condition, using a system of Solartron SI 1260 and 1287 (Electrochemical interface, the United Kingdom). The impedance spectra were analyzed using equivalent circuit models by Zview fitting software.

Results and analysis

Fabrication of Transparent Leaf-like Cu₂ZnSnS₄ (CZTS) Plate Arrays (PLAr)

The fabrication process of leaf-like CZTS PLAr CE is schematically indicated in Figure 1. There are two stages in the preparation of high-performance and low-cost CZTS CE. A precursor metallic film composed of Cu, Sn, and Zn is firstly electrodeposited on a FTO glass substrate under potentiostatic control without stirring. Then the precursor CZT film is under solvothermal treatment in a sealed autoclave containing sulfur powders and ethanol for 6 h. It is mentioned in previous studies that homogeneous deposition of the metallic precursor is important to obtain a compact and robust multi-metal sulfide film.²³⁻²⁶ Hence, various parameters (such as concentrations and potential) for electrodeposition of metallic elements were adjusted, specifically for Sn and Zn deposition. Because the Sn prefers to form a lump morphology and the Zn tends to become an island shape most likely due to the side reaction of H₂ evolution. As reported in the experimental section, we finally achieved the best conditions.

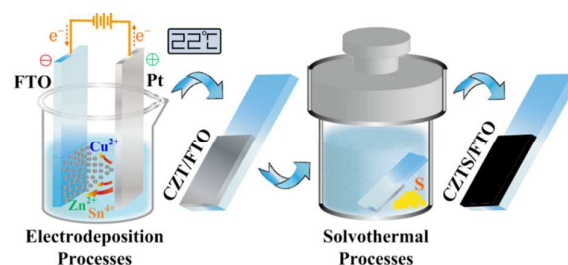


Figure 1. Schematic illustration of the fabrication processes of Cu₂ZnSnS₄ counter electrode.

Optical and field-emission scanning electron microscope (FE-SEM) images of the as-prepared CZTS films are presented in Figure 2. It is apparent that all the films on FTO substrate are semi-transparent from the optical images. The excellent transmittance suggests the CZTS film potential for more light coming into the cells from counter electrode, so as to improve the photovoltaic performance. After the CZT precursor film

transforming to CZTS, the color changes from light brown to dark brown, as the CZTS phase can absorb the visible light ranging from ca. 400–800 nm. The resulting CZTS film shows a ca. \sim 350 nm thick homogeneous and compact layer. Moreover, the whole FTO substrate is uniformly covered by solvothermal-synthesized leaf-like CZTS PLAR with width of ca. \sim 350 nm and thickness of ca. \sim 30 nm. The surface of CZTS plate is extremely rough and composed of numerous pyramidal nanoparticles with expanding specific surface area, as shown in Figure 2 (d) and S1. This unique leaf-like structure is beneficial to higher catalytic activity, as more and more electrolyte can adsorb on the CZTS PLAR and the photo-generated electrons can transfer through the plate arrays into the conductive substrate quickly and effectively. Notably, all the elements are homogeneously distributed over a single CZTS plate (Figure 4 (e,f)).

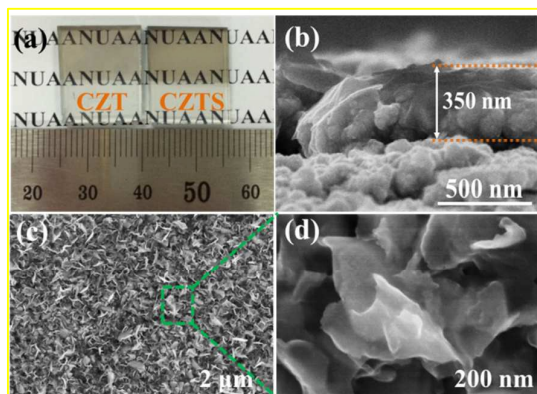


Figure 2. (a) Digital photograph of CZT film and CZTS counter electrode on the FTO substrate. (b) Cross-sectional FE-SEM image of the CZTS film, slightly detached from the glass substrate due to sample preparation. (c,d) FE-SEM images of leaf-like CZTS arrays on FTO substrate.

The phase-structural properties of the as-synthesized CZTS CE are illustrated in Figure 3. The observed diffraction peaks show that kesterite-structure CZTS films (JCPDS 26-0575) are obtained during solvothermal treatment. The three strong diffraction peaks around 28.5° , 32.9° , and 47.3° are assigned to those crystal faces of (112), (200), and (220) respectively. Furthermore, it is noteworthy that the XRD profiles of tetragonal Cu_2SnS_3 (JCPDS 89-4714) and cubic ZnS (JCPDS 80-0020) are similar to that of kesterite CZTS phase.^{15,18,27} The further structural information of the sample on macroscopic scale is obtained from Raman spectrum. The peaks from Cu_2SnS_3 (352 cm^{-1}), ZnS (346 cm^{-1}), and Cu_{2-x}S (475 cm^{-1}) phases are not observed in Figure 3 (b). The biggest Raman peak at 338 cm^{-1} are from kesterite CZTS phase.¹⁵ These results exclude the presence of other binary or ternary sulfide compounds, with only CZTS existing, which are similar to those in previous reports.^{15,27} Hence, the pure kesterite-structure CZTS CE is obtained through novel solvothermal treatment for 6 h.

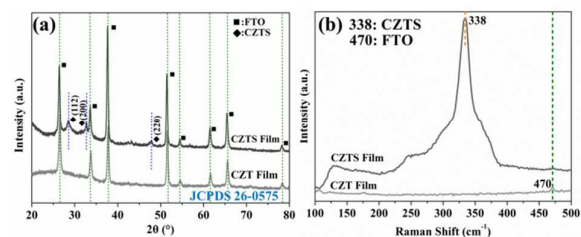


Figure 3. (a) XRD patterns and (b) Raman spectra of the as-synthesized CZT film and CZTS CE on FTO substrate, exhibiting the well-defined signals assigned to the deflections of the lattice facets in the kesterite-structure CZTS phase (JCPDS no. 26-0575). It is noted that the thicker CZTS film for Raman characterization was fabricated with the CZT electrodeposition time extension to 10 min.

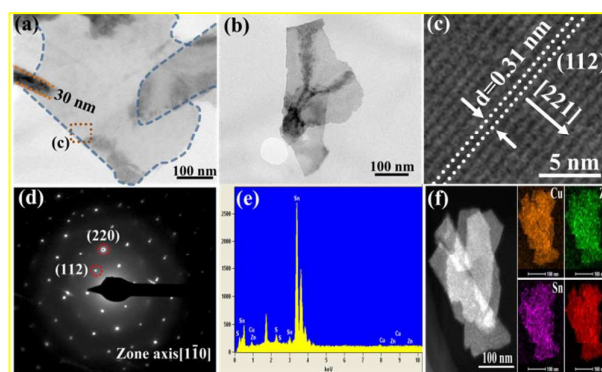


Figure 4. (a,b) TEM images of the leaf-like CZTS plate grown on the FTO substrate by solvothermal treatment. (c) HR-TEM image and (d) SAED pattern of a single plate scraped from the films of CZTS arrays. (e) EDS dot spectrum for CZTS. (f) Dark field TEM image of CZTS plate and EDS elemental mapping of Cu, Zn, Sn, and S.

To further study the detailed structures of the products, TEM measurement was subsequently performed. The light contrast in various areas of the TEM image indicates the thin two-dimensional (2D) nature of the plate-like nanostructures. Besides, the curled edge shows that the CZTS plates are composed of multiple layers with a thickness of ca. 30 nm (also confirmed by the AFM image in Figure S2, demonstrating a thickness of 30–40 nm), further verifying the ultrathin nature of the CZTS plates. HR-TEM image shows crystallographic plane clearly. The plane represents one set of d-spacing, namely of 0.31 nm, which corresponds to the (112) planes of kesterite-structure CZTS. The corresponding selected-area electron diffraction (SAED) pattern of the tetragonal-structure CZTS plate displays several diffraction dots, demonstrating that it is single crystals with great crystallinity. The presence of the major diffraction dots (112) and (220) is in good agreement with those reported in the literature.^{22,28} No apparent

additional sulfide phases are observed and the pure phase of the CZTS film is further confirmed.

To verify the universality and efficiency of the novel solvothermal treatment in synthesizing different nanostructure and multi-metal sulfides, we extended the method to CZTS nanodisk arrays fabrication, by choosing sodium thiosulfate as the starting sulfur source. In the first step, CZT precursor film was similarly electrodeposited on FTO glass substrate, with the morphology of nanoparticles. During the solvothermal treatment, the CZT composite changes to CZTS phase and nanodisk architecture is well formed (as shown in Figure S3). The as-prepared CZTS sheet surfaces are rough, with abundant nanoparticles covering on it. The thickness and diameter of the CZTS nanodisk is ca. 30-70 nm and ca. 300-500 nm, respectively. Raman spectra confirm the conversion from CZT precursor to CZTS. TEM result indicates that the obtained nanodisk CZTS exhibits single crystal structure, with the diffraction dots appearing in Figure S3 (c). The measured lattice fringe with an interplane spacing of 0.312 nm in the HR-TEM image corresponds to the (112) plane of kesterite-structure CZTS phase. Furthermore, we also obtained Cu_4SnS_6 sheet arrays when the Cu-Sn alloy composite was firstly electrodeposited on FTO glass substrate and sulphur served as the sulfur source. The thickness and width of the Cu_4SnS_6 sheet is ca. 20-40 nm and ca. 350-580 nm, respectively (as demonstrated in Figure S4). The EDS spectra and XRD data confirm the Cu_4SnS_6 formation. All in all, the above demonstrations serve as strong testament that this green solvothermal treatment is powerful and versatile for constructing high-quality metal sulfide nanoarrays on arbitrary conductive substrates under mild condition (i.e. low temperature, no annealing, environment, speediness).

Reaction Mechanism

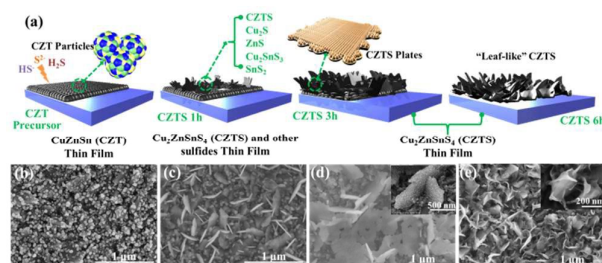


Figure 5. (a) Schematic illustration of the growth mechanism of the conversion process from CZT particles to leaf-like CZTS plate arrays on FTO substrate. FE-SEM images of the films of (b) CZT, (c) CZTS 1 h, (d) CZTS 3 h, and (e) CZTS 6 h.

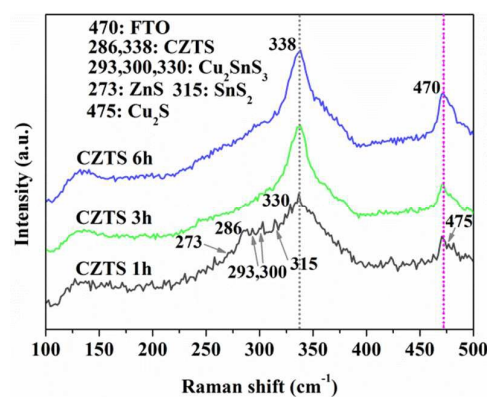


Figure 6. Structural characterizations of the as-fabricated CZTS films obtained at various conversion periods.

The growth mechanism of the 2D leaf-like CZTS PLAR based on solvothermal treatment is proposed as follows (also shown schematically in Figure 5 (a)). The morphology evolution of CZTS during the solvothermal process is examined by FE-SEM characterizations. From Figure 5 (a) and (b), the porous and rough precursor CZT film before the solvothermal treatment is composed of homogeneous particles, with the diameter of 50-65 nm. Interestingly, in the first conversion process for 1 h, many irregular nanoplates appear, however with abundant of particles remaining. Most likely, it is due to the "oriented attachment" and "self-assembly" processes²⁹⁻³¹ which involve a spontaneous self-organization of adjacent particles so that they share a common crystallographic orientation, followed by joining of these particles at a planar interface. The processes are particularly relevant in the nanocrystalline regime, where bonding between the adjacent particles reduces overall energy by removing surface energy associated with unsatisfied bonds.^{29,32,33} Furthermore, during the solvothermal process, sulfur powders dissolves in trace amount of water to form H_2S and is also further decomposed to S^{2-} species, namely as disproportionation.^{34,35} The released species can serve as the sulfur sources in solvothermal treatment to convert CZT precursor to CZTS phase. In addition, the surface of the rough CZT film has many small grain boundaries and ethanol and the above sulfur species can easily permeate into the film to react with CZT compound to form sulfide at a low temperature and high pressure. As shown in Figure 6, Cu_2S , ZnS , SnS_2 , Cu-Zn-Sn , and CZTS composite phases are initially formed in the shape of nanoplate and nanoparticle, acting as the starting crystal nucleus of CZTS plate arrays. It is proposed that the formation of CZTS nanoplate involves nucleation and growth, described in previous reports.³⁶ With the reaction proceeding to 3 h, the binary/ternary sulfide continue to react with each other and the sulfur species to form kesterite-structure $\text{Cu}_2\text{ZnSnS}_4$ phase and there are not any impurity phases left, as observed in Figure 6. Moreover, as shown in Figure S5, the dark-field TEM imaging clearly shows that a growing CZTS plate is composed of abundant tiny nanocrystals. The adjacent nanocrystals share

similar growth orientation ([221] direction), and then combine each other to form a whole single-crystal plate with reaction time extension. For CZTS 3 h sample, the width for each plate increases from ca. ~ 300 nm to ca. ~ 600 nm and the surface is getting rougher. The mosaic and rough pointed cone on the surface of plate can provide high-energy sites for crystal growth (seeing in Figure S5 (b)). It is energetically more favorable for the crystalline CZTS plates to grow, where they evolve from small nanoplate to well-defined interconnected bigger CZTS plates with sawtooth-structured protuberances (namely as Ostwald ripening process). When the reaction time is 6 h, it is noteworthy that the CZTS plate becomes thinner, with the smooth edge of the plate curling up and becoming cambered. It is hypothesized that the redundant S^{2-} ions or H_2S species absorb on the surface or active site of the CZTS plate, and then the above active species react with the surface layer and boundary of the CZTS further, so as to minimize the surface energy and acquire better crystalline (as proved in Figure 6). Thus, the leaf-like CZTS PLAR with high specific surface area and super crystalline is prefer to be obtained.

Performance of DSSCs and Electrochemical Properties of Leaf-like CZTS PLAR CE

Photocurrent density-voltage (J-V) curves of DSSCs using CEs based on conventional Pt, and different CZTS thin films were obtained under a light intensity of 100 mW/cm^2 . The photovoltaic parameters are listed in Table 1 and each value for cell performance is determined as an average of at least three devices. It is indicated that the DSSCs with leaf-like CZTS 6h PLAR CE possess a much better cell performance than others, especially for the J_{SC} . The significantly enhanced J_{SC} values indicate that the rate of hole recovery at the CZTS 6h PLAR electrode-electrolyte interface is more rapid than that at the other CEs.^{9,37} A 7.09 % efficiency is successfully achieved with leaf-like CZTS 6h PLAR CE, which is about 18 % times higher than that of Pt CE-based DSSCs ($\eta=6.01$ %). As a high-efficiency catalyst for the reduction of I_3^- , CZTS 6h PLAR CE demonstrates great potential application in DSSCs. The higher J_{SC} and FF of the CZTS 6h CE are due to the considerable improvement in charge transfer at the CE/electrolyte interface, which reduces the internal resistances, the concentration gradients in the electrolyte, and the recombination rates.^{38,39} Furthermore, a reflective mirror was used to improve the visible light utilization rate of the CZTS 6h CE to achieve high transmittance, as shown in Figure 7. Surprisingly, the J_{SC} increases from 16.32 to 21.78 mA/cm^2 , when reflecting the light penetrating through the solar cell, and the PCE increases from 7.09 % to 8.67 % accordingly. The superior catalytic ability of leaf-like CZTS PLAR in DSSCs could be caused by the following reason: First, plate-based catalytic arrays not only increase catalytic surface area of electrode films but also accelerate the photo-generated electron transport at the counter electrode/redox electrolyte interface;^{16,40} Second, according to the quantum chemistry predictions, the (202)

surface of metal sulfide has overpotential behavior in O_2 reduction similar to that observed for platinum electrodes, indicating the special surface structure of metal sulfide benefits the reduction of I_3^- ions.⁴¹ However, the PCE of the CZTS 1h device (5.10 %) was lower than that of Pt counter electrode. This could be due to the presence of the secondary phase like Cu_2SnS_3 , ZnS , SnS_2 and Cu_2S phases (observed in Raman spectra), which have been shown to have poor catalytic activity in iodine/iodide electrolyte and served as electron recombination sites.^{22,42}

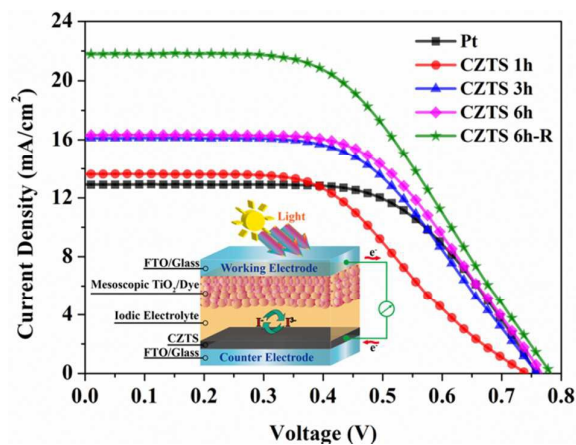


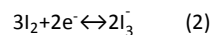
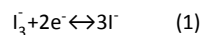
Figure 7. J-V characteristics of DSSCs with Pt and different transparent CZTS films as CEs under a light intensity of 100 mW/cm^2 (1 sun). The inset shows the schematic structure of the DSSCs device by using semi-transparent CZTS films as a counter electrode.

Table 1. Photovoltaic parameters for DSSCs assembled with Pt and CZTS CEs.

CE	J_{SC} (mA/cm^2)	V_{OC} (V)	FF (%)	PCE (%)
CZTS 1h	13.62 ± 0.53	0.73 ± 0.02	51.18 ± 0.03	5.10 ± 0.22
	16.11 ± 0.45	0.75 ± 0.01	55.70 ± 0.05	6.75 ± 0.18
CZTS 3h	16.32 ± 0.38	0.76 ± 0.01	57.21 ± 0.02	7.09 ± 0.37
	21.78 ± 0.43	0.78 ± 0.01	51.07 ± 0.01	8.67 ± 0.33
CZTS 6h-R	12.90 ± 0.52	0.75 ± 0.02	61.42 ± 0.03	6.01 ± 0.28

The observed cell performance enhancement is further investigated by evaluating the electrocatalytic activity of the CZTS and Pt electrode and the electrochemical impedance spectroscopy (EIS), cyclic voltammetry (CV) and Tafel-polarization measurements were performed in triiodide electrolyte. Figure 8 (a) shows that leaf-like CZTS PLAR CE has excellent electrochemical stability in I^-/I_3^- solutions. Two pairs of oxidation and reduction peaks are observed in CV curves for

all samples. The redox peaks at more negative potentials, represented by peak I and peak I', correspond to the reaction of eqn 1, and the redox peaks at more positive potentials, represented by peak II and peak II', correspond to eqn 2:^{16,43,44}



As the counter electrode of DSSCs is responsible for catalyzing the reduction of I_3^- to I^- , the characteristics of peak I and peak I' are the focus of our analysis. The cathodic peak current (I_p) at more negative potential and the peak-to-peak separation (ΔE_p), which is negatively correlated with the standard electrochemical rate constant of the redox reaction, are two critical parameters for comparing electrocatalytic activities of different CEs.⁴⁴ Compared to Pt electrode, though the value of ΔE_p (0.72 V) for CZTS 6h is nearly comparable to that of the Pt (0.71 V), the peak position of reduction reaction is shifted from -0.49 to -0.55 V. The shift of the reduction peaks toward the negative potentials indicates that the oxidized iodide species, which are formed by scavenging the photoexcited holes of the dye, are easily reduced and regenerated on the counter electrode coated with the heterostructured nanostructure.⁴⁴ The higher I_p of CZTS 6h at peak I indicates that the leaf-like CZTS PLAR CE produces remarkable catalytic activity for I_3^- reduction, even better than Pt, which is advantageous for the application of the CZTS material as an efficient CE in DSSCs. Furthermore, the catalytic reaction is a kinetic process, which is related to the electron transfer rate constant and the number of active sites. Peak I' is wider for the leaf-like CZTS PLAR electrode than that for Pt, which indicates that the 2D CZTS PLAR structure has provided more catalytic reaction sites than the Pt CE.⁹ Thus, the 2D leaf-like CZTS PLAR CE has superior catalytic activity properties compared to Pt. The conclusion from the CV data is consistent with previous energy conversion efficiency results.

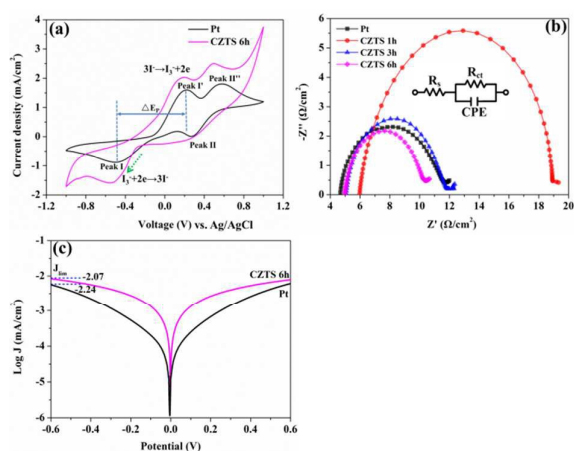


Figure 8. (a) Cyclic voltammograms of Pt and CZTS 6h electrodes measured in an acetonitrile solution containing 1 mM I_2 , 10 mM LiI, and 0.1 M $LiClO_4$ at a scan rate of 100 mV/s. (b) Nyquist plots for the I_3^-/I^- symmetrical cells based on Pt and various CZTS CEs under a

bias of 0 V. (c) Tafel plots of Pt and CZTS 6h symmetrical cells between ± 1.0 V with a scan rate of 10 mV at room temperature. The inset shows equivalent circuit diagram for the symmetrical cells.

Table 2. Electrochemical parameters of Pt and CZTS CEs.

CE	R_s (Ω/cm^2)	R_{ct} (Ω/cm^2)	C_μ (μF)	ΔE_p (V)
CZTS 1h	5.98	13.17	7.41	/
CZTS 3h	5.05	6.64	14.65	/
CZTS 6h	4.98	5.29	17.24	0.72
Pt	4.67	7.17	13.92	0.71

To further elucidate the catalytic activity of the CZTS CEs in the reduction of I_3^- ions, electrochemical impedance spectroscopy (EIS) was conducted on the symmetrical CZTS and Pt electrochemical cells, as shown in Figure 8 (b). Generally, the high frequency intercepts on the real axis represent the series resistance (R_s), which is mainly composed of the bulk resistance of CE materials, resistance of FTO glass substrates, contact resistance, etc. The high frequency semicircle indicates the electrochemical charge transfer resistance (R_{ct}) parallel with the corresponding double-layer capacitance (C_μ) at the interface of CE/electrolyte for I_3^- reduction. The detailed EIS parameters are listed in Table 2. The R_s values of the CZTS 1h, CZTS 3h and CZTS 6h CEs are 5.98, 5.05, and 4.98 Ω/cm^2 , respectively, which are comparative to that of the Pt electrode (4.67 Ω/cm^2). The small value of CZTS CEs reflects a good bonding strength between in-situ CZTS films and FTO substrate, which in turn promotes the transfer of more electrons from the external circuit or of holes from the electrolyte to the CEs.⁴⁵ The R_s greatly affects the FF and J_{sc} of the solar cell, with higher FF and J_{sc} resulting from smaller R_s value, which is consistent with the result of photovoltaic performance.⁴⁵ The CZTS 6h electrode exhibits the smallest R_{ct} value of 5.29 Ω/cm^2 , indicating an acceleration of high electron transfer at the interface of CE/electrolyte and high catalytic activity, thus leading to higher J_{sc} and FF.^{8,46,47} The small value of R_{ct} is due to the high contact surface area and fast electron-transfer pathway of CZTS PLAR.⁴⁷ Furthermore, a higher C_μ value (17.24 μF) represents a larger surface area of the CZTS 6h, which agrees well with the results obtained from the FE-SEM and AFM analyses.^{45,48} Accordingly, the leaf-like CZTS PLAR CE shows higher active catalytic properties than Pt for the reduction of I_3^- , which agrees well with the CV results. For CZTS 3h CE, the corresponding R_{ct} value is 6.64 Ω/cm^2 , which is comparative to that of the Pt CE. However, it can be observed that the R_{ct} value (13.17 Ω/cm^2) for the CZTS 1h is larger than 7.17 Ω/cm^2 , indicating the poor electrocatalytic activity as evidenced by the J-V characteristics of DSSCs.

In addition, Tafel polarization measurement was also carried out with the same symmetrical cells in the above EIS test to further investigate the electrocatalytic activity of the CZTS 6h and Pt CE. It is a measurement of logarithmic current density (Log J) as a function of applied potential. The Tafel plot consists of three zones: the first one is the polarization zone at the lower potential (-V), the

second one is the Tafel zone at the middle with a steep slope, which is the fingerprint of catalytic ability of the CE, and the third one is due to diffusion region at the higher voltage (V).^{49,50} The exchange current density (J_0) of samples can be evaluated as the intercept of the extrapolated linear region of anodic and cathodic branches when the voltage is zero. It can be seen in Figure 8 (c) that the CE with CZTS 6h shows the higher J_0 than Pt, suggesting the better electrocatalytic activity, in good agreement with the tendency of the cathodic peak current observed in Figure 8 (a).⁹ The J_0 value is directly related to the charge transfer resistance (R_{ct}) and is given by the following eqn 3:

$$J_0 = RT/nFR_{ct} \quad (3)$$

where R is the gas constant, T is the absolute temperature in K, n is the number of electrons involved in the electrochemical reduction reaction, F is the Faraday constant, and R_{ct} is the charge transfer resistance at the CE/electrolyte interface obtained from EIS spectra.⁵¹⁻⁵⁴ Therefore, the J_0 value is proportional to the R_{ct} value. The limiting diffusion current density (J_{lim}) can be also derived from the Tafel curve at high potential. J_{lim} is closely related to the catalytic activity of the catalyst.^{9,45,55} The J_{lim} value of the leaf-like CZTS PLAR electrode (-2.07 mA/cm^2) is higher than that of the Pt electrode (-2.24 mA/cm^2), which induces a higher diffusion coefficient, as shown in eqn 4.^{10,52} J_{lim} depends on the diffusion coefficient of the redox couple in the electrolyte. This Tafel polarization result is consistent with the EIS and CV results.

$$D = lJ_{lim}/2nFC \quad (4)$$

where D is the diffusion coefficient of the I_3^- , l is the electrolyte thickness, n is the number of electrons involved in the reduction of I_3^- at the counter electrode, F is the Faraday constant, and C is the iodic concentration.

Conclusions

In summary, we have demonstrated a green, effective and powerful two-step method based on novel solvothermal treatment to synthesize semi-transparent 2D leaf-like CZTS PLAR in situ on FTO glass substrate. The electrodeposited CZT precursor film was completely converted to leaf-like CZTS PLAR after a solvothermal treatment in the period of 6 h. The corresponding SAED pattern of the tetragonal-structure CZTS plate demonstrated its single crystals with great crystallinity. The growth mechanism is related to the "oriented attachment" and "self-assembly" processes. The dissolved S^{2-} ions and hydrolyzed H_2S species serve as the sulfur sources in solvothermal treatment to convert CZT precursor to CZTS. Remarkably, power conversion efficiency (PCE) of 7.09 % was obtained by utilizing leaf-like CZTS PLAR as CE for DSSCs, which was higher than that of Pt (6.01 %). Surprisingly, PCE increased to 8.67 % under assisted by a mirror. The excellent performance of DSSCs could be attributed to high catalytic surface area, fast photo-generated electron transport at the counter electrode/redox electrolyte interface, remarkable electrocatalytic activity for I_3^- reduction, low charge transfer

resistance toward the reduction of I_3^- ions, and high diffusion coefficient of the I_3^- . This work provides a green and feasible approach to construct high-quality metal sulfide nanoarrays on arbitrary substrates under mild condition (i.e. low temperature, no annealing, environment, speediness) and promotes the development of sulfide materials for solar cells, photo/electro-catalysis, and electrochemical energy storage applications.

Acknowledgements

The authors are thankful for the support from the National Nature Science Foundation of China (Grant no. 51202112), the Priority Academic Program Development of Jiangsu Higher Education Institutions (PAPD), the Foundation of Graduate Innovation Center in NUAA (Grant no. KFJJ201442), the Fundamental Research Funds for the Central Universities (Grant no. NJ20150027), and the Open Fund of Jiangsu Key Laboratory of Materials and Technology for Energy Conversion (Grant no. MTEC-2015M04).

Notes and references

- 1 K. Anderson, A. Bows and Philos, *Trans. R. Soc. A*, 2011, **369**, 20-44.
- 2 M.M. Lee, J. Teuscher, T. Miyasaka, T.N. Murakami and H.J. Snaith, *Science*, 2012, **338**, 643-647.
- 3 C.K. Chan, H.L. Peng, G. Liu, K. McIlwrath, X.F. Zhang, R.A. Huggins and Y. Cui, *Nat. Nanotechnol.*, 2008, **3**, 31-35.
- 4 B. O'Regan and M. Gratzel, *Nature*, 1991, **353**, 737-740.
- 5 P. Docampo, S. Guldin, T. Leijtens, N.K. Noel, U. Steiner and H.J. Snaith, *Adv. Mater.*, 2014, **26**, 4013-4030.
- 6 S. Mathew, A. Yella, P. Gao, R. Humphry-Baker, B.F.E. Curchod, N. Ashari-Astani, I. Tavernelli, U. Rothlisberger, K. Nazeeruddin Md and M. Grätzel, *Nat. Chem.*, 2014, **6**, 242-247.
- 7 M.I. Asghar, K. Miettunen, J. Halme, P. Vahermaa, M. Toivola, K. Aitola and P. Lund, *Energy Environ. Sci.*, 2010, **3**, 418-426.
- 8 S. Thomas, T.G. Deepak, G.S. Anjusree, T.A. Arun, S.V. Naira and A.S. Nair, *J. Mater. Chem.*, 2014, **2**, 4474-4490.
- 9 J. Ma, C. Li, F. Yu and J. Chen, *ChemSusChem*, 2014, **7**, 3304-3311.
- 10 Y. Xiao, J. Wu, J. Lin, G. Yue, J. Lin, M. Huang, Y. Huang, Z. Lan and L. Fan, *J. Mater. Chem. A*, 2013, **1**, 13885-13889.
- 11 G. Liu, H. Wang, X. Li, Y. Rong, Z. Ku, M. Xu, L. Liu, M. Hu, Y. Yang, P. Xiang, T. Shu and H. Han, *Electrochim. Acta*, 2012, **69**, 334-339.
- 12 G. Veerappan, K. Bojan and S.W. Rhee, *ACS Appl. Mater. Inter.*, 2011, **3**, 857-862.
- 13 S.S. Rao, C.V.V.M. Gopi, S.K. Kim, M.K. Son, M.S. Jeong, A.D. Savariraj, K. Prabakar and H.J. Kim, *Electrochim. Acta*, 2014, **133**, 174-179.
- 14 X. Xin, M. He, W. Han, J. Jung and Z. Lin, *Angew. Chem., Int. Ed.*, 2011, **50**, 11739-11742.
- 15 Y.L. Zhou, W.H. Zhou, M. Li, Y.F. Du and S.X. Wu, *J. Phys. Chem. C*, 2011, **115**, 19632-19639.
- 16 Y. Liao, K. Pan, Q. Pan, G. Wang, W. Zhou and H. Fu, *Nanoscale*, 2015, **7**, 1623-1626.
- 17 Y. Liu, Y. Xie, H. Cui, W. Zhao, C. Yang, Y. Wang, F. Huang and N. Dai, *Phys. Chem. Chem. Phys.*, 2013, **15**, 4496-4499.
- 18 Y. Xie, C. Zhang, F. Yue, Y. Zhang, Y. Shi and T. Ma, *RSC Adv.*, 2013, **3**, 23264-23268.

- 19 Y.F. Du, J.Q. Fan, W.H. Zhou, Z.J. Zhou, J. Jiao and S.X. Wu, *ACS Appl. Mater. Inter.*, 2012, **4**, 1796-1802.
- 20 Z. Tong, Z. Su, F. Liu, L. Jiang, Y. Lai, J. Li and Y. Liu, *Mater. Lett.*, 2014, **121**, 241-243.
- 21 P. Dai, G. Zhang, Y. Chen, H. Jiang, Z. Feng, Z. Lin and J. Zhan, *Chem. Commun.*, 2012, **48**, 3006-3008.
- 22 S. Wozny, K. Wang and W. Zhou, *J. Mater. Chem. A*, 2013, **1**, 15517-15523.
- 23 X. Yin, Z. Xue and B. Liu, *J. Power Sources*, 2011, **196**, 2422-2426.
- 24 S.M. Lee, S. Ikeda, Y. Otsuka, W. Septina, T. Harada and M. Matsumura, *Electrochim. Acta*, 2012, **79**, 189-196.
- 25 F. Jiang, S. Ikeda, T. Harada and M. Matsumura, *Adv. Energy Mater.*, 2014, **4**, 1301381.
- 26 Y. Li, T. Yuan, L. Jiang, Z. Su and F. Liu, *J. Alloy. Compd.*, 2014, **610**, 331-336.
- 27 C. Zou, L. Zhang, D. Lin, Y. Yang, Q. Li, X. Xu, X. Chen and S. Huang, *CrystEngComm*, 2011, **13**, 3310-3313.
- 28 J. Xu, X. Yang, Q.D. Yang, T.L. Wong and C.S. Lee, *J. Phys. Chem. C*, 2012, **116**, 19718-19723.
- 29 L.Q. Mai, F. Yang, Y.L. Zhao, X. Xu, L. Xu and Y.Z. Luo, *Nat. Commun.*, 2011, **2**, 381.
- 30 H. Colfen and M. Antonietti, *Angew. Chem., Int. Ed.*, 2005, **44**, 5576-5591.
- 31 R.L. Penn and J.F. Banfield, *Science*, 1998, **281**, 969-971.
- 32 M. Niederberger and H. Colfen, *Phys. Chem. Chem. Phys.*, 2006, **8**, 3271-3287.
- 33 X. Xia, J. Tu, Y. Zhang, X. Wang, C. Gu, X. Zhao and H.J. Fan, *ACS Nano*, 2012, **6**, 5531-5538.
- 34 Z. Qiu, H. Lian, Ti. Luo, J. Fan, X. Cai, Z. Cheng, M. Shang, S. Lian and J. Lin, *CrystEngComm*, 2015, **17**, 8676-8682.
- 35 S. Liu, M. Li, S. Li, H. Li and L. Yan, *Appl. Surf. Sci.*, 2013, **268**, 213-217.
- 36 M.D. Regulacio, C. Ye, S.H. Lim, M. Bosman, E. Ye, S. Chen, Q.H. Xu and M.Y. Han, *Chem.-Eur. J.*, 2012, **18**, 3127-3131.
- 37 W. Guo, X. Zhang, R. Yu, M. Que, Z. Zhang, Z. Wang, Q. Hua, C. Wang, Z.L. Wang and C. Pan, *Adv. Energy Mater.*, 2015, **5**, 1500141.
- 38 T.W. Hamann, R.A. Jensen, A.B.F. Martinson, H. Van Ryswyk and J.T. Hupp, *Energy Environ. Sci.*, 2008, **1**, 66-78.
- 39 H.J. Kim, S.W. Kim, C.V.V.M. Gopi, S.K. Kim, S.S. Rao and M.S. Jeong, *J. Power Sources*, 2014, **268**, 163-170.
- 40 X. Miao, K. Pan, G. Wang, Y. Liao, L. Wang, W. Zhou, B. Jiang, Q. Pan and G. Tian, *Chem.-Eur. J.*, 2014, **20**, 474-482.
- 41 E. Vayner, R.A. Sidik and A.B. Anderson, *J. Phys. Chem. C*, 2007, **111**, 10508-10513.
- 42 S. Das, P. Sudhagar, S. Nagarajan, E. Ito, S.Y. Lee, Y.S. Kang and W. Choi, *Carbon*, 2012, **50**, 4815-4821.
- 43 L. Yi, Y. Liu, N. Yang, Z. Tang, H. Zhao, G. Ma, Z. Su and D. Wang, *Energ. Environ. Sci.*, 2013, **6**, 835-840.
- 44 W. Wang, X. Pan, W. Liu, B. Zhang, H. Chen, X. Fang, J. Yao and S. Dai, *Chem. Commun.*, 2014, **50**, 2618-2620.
- 45 C.V.V.M. Gopi, S.S. Rao, S.K. Kim, D. Punnoose and H.J. Kim, *J. Power Sources*, 2015, **275**, 547-556.
- 46 T. Ma, X. Fang, M. Akiyama, K. Inoue, H. Noma and E. Abe, *J. Electroanal. Chem.*, 2004, **574**, 77-83.
- 47 M.S. Fan, J.H. Chen, C.T. Li, K.W. Cheng and K.C. Ho, *J. Mater. Chem. A*, 2015, **3**, 562-569.
- 48 G.R. Li, F. Wang, Q.W. Jiang, X.P. Gao and P.W. Shen, *Angew. Chem. Int. Ed.*, 2010, **49**, 3653-3656.
- 49 A.D. Savariraj, K.K. Viswanathan and K. Prabakar, *ACS Appl. Mater. Inter.*, 2014, **6**, 19702-19709.
- 50 M.J. Ju, J.C. Kim, H.J. Choi, I.T. Choi, S.G. Kim, K. Lim, J. Ko, J.J. Lee, I.Y. Jeon, J.B. Baek and H.K. Kim, *ACS Nano*, 2013, **7**, 5243-5250.
- 51 J. Dong, S. Jia, J. Chen, B. Li, J. Zheng, J. Zhao, Z. Wang and Z. Zhu, *J. Mater. Chem.*, 2012, **22**, 9745-9750.
- 52 M. Wang, A.M. Anghel, B. Marsan, N.L. Cevey Ha, N. Pootrakulchote, S.M. Zakeeruddin and M.J. Grätzel, *J. Am. Chem. Soc.*, 2009, **131**, 15976-15977.
- 53 A. Hauch and A. Georg, *Electrochim. Acta*, 2001, **46**, 3457-3466.
- 54 A. Banerjee, K.K. Upadhyay, S. Bhatnagar, M. Tathavadekar, U. Bansode, S. Agarkar and S.B. Ogale, *RSC Adv.*, 2014, **4**, 8289-8294.
- 55 M.X. Wu, X.A. Lin, A. Hagfeldt and T.L. Ma, *Angew. Chem. Int. Ed.*, 2011, **50**, 3520-3524.

Graphical abstract

